*Int. J. Multiphase Flow* Vol. 12, No. 5, pp. 791–806, 1986
Printed in Great Britain. 

0301-9322/86 $3.00 + 0.00


# A TWO-DIMENSIONAL MODEL OF THE FLOW OF ORDERED SUSPENSIONS OF RODS

J. H. MASLIYAH† and T. G. M. VAN DE VEN
Pulp & Paper Research Institute of Canada and Department of Chemistry, McGill University, Montreal, Quebec H3A 2A7, Canada

(*Received* 21 *June* 1985; *in revised form* 17 *November* 1985)

**Abstract**—Analysis of creeping flow over an array of freely-rotating cylinders sandwiched between two sliding parallel plates is studied using a finite-difference and a least-squares numerical technique. The flow pattern was found to be very much influenced by the cylinder-to-cylinder spacing and by the gap width of the parallel plates. The shear stress on the cylinder surface and on the parallel plates was found to be a strong function of position. The viscosity of a suspension composed of an array of freely-rotating cylinders was deduced from the applied shear rate and the evaluated shear stress on the parallel plates. Experimental results confirm the numerical findings.

## INTRODUCTION

Suspensions of particles can exhibit ordered structures, especially in the case of monodisperse particles at sufficiently high volume fractions. The best-known example is probably an aqueous suspension of tobacco virus particles which, with increasing volume fraction, changes from isotropic to birefringent and finally into an iridescent gel (Oster 1950; Forsyth *et al.* 1978). These phenomena clearly show that the tobacco mosaic virus particles align themselves at higher volume fractions. The same phenomena occur with suspensions of spherical particles, which usually settle into a hexagonally-packed layer structure (Hiltner *et al.* 1971; Tomita *et al.* 1983). The phase transitions of disordered to ordered structures have been explained theoretically (Onsager 1949; Alder *et al.* 1968).

It is of interest to consider what happens when such ordered structures are subjected to shear. It has been shown (Hoffman 1974) that sheared ordered suspensions of spheres consist of a stack of layers that slide over each other. Recently (Tomita & van de Ven 1984), it has been found that the distance between these sliding layers depends on the rate of shear, the distance being larger at higher shear rates. This implies that ordered suspensions of spheres restructure themselves when subjected to shear; they settle in fewer more densely packed layers with increasing shear. Similar phenomena can be expected for suspensions of anisometric particles (van de Ven 1985).

A precise description of the flow around particles in sheared ordered suspensions is extremely complicated. Such studies were made by Zuzovsky *et al.* (1983), Adler & Brenner (1985) and Adler *et al.* (1985). A useful simplification that can be made is to consider only one layer of particles that is being sheared between two solid plates. The behavior of particles in such a layer can be expected to be qualitatively similar to that of a layer in an ordered suspension, except that the nonsteady periodic character of the flow is replaced by an averaged steady flow.

In this paper we consider the simplest case, namely the flow around an array of aligned infinitely long cylinders subjected to shear. We believe the results will be relevant to the flow of ordered suspensions of rods. In the following sections we describe the governing equations, methods for solving them, results of numerical calculations and, finally, the results of experiments that confirm certain aspects of the theory.

†On leave from the University of Alberta, Edmonton, Alberta, Canada.

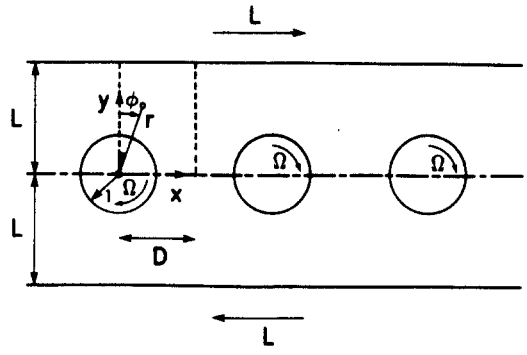


Figure 1. Flow geometry.

## GOVERNING EQUATIONS

Creeping flow of a Newtonian fluid over an array of circular cylinders sandwiched between two parallel plates moving in opposite directions is governed by

$$\nabla^4\psi = 0, \qquad [1]$$

where $\psi$ is the dimensionless stream function and

$$\nabla^2 = \frac{\partial^2}{\partial r^2} + \frac{1}{r}\frac{\partial}{\partial r} + \frac{1}{r^2}\frac{\partial^2}{\partial \phi^2}. \qquad [2]$$

Here $r$ is the distance from the center of a reference cylinder, normalized by the cylinder radius $R$ and $\phi$ is the polar angle (see figure 1). The biharmonic flow equation [1] can be written as

$$\nabla^2\psi = \zeta \qquad [3a]$$

and

$$\nabla^2\zeta = 0, \qquad [3b]$$

where $\zeta$ is the flow vorticity. Using the cylinder radius as the characteristic length and a suitable angular velocity $\Omega^*$ as the characteristic reciprocal time, the following quantities were rendered dimensionless:

$$\psi = \psi'/R^2\Omega^*, \quad \zeta = \zeta'/\Omega^*, \quad L = L'/R, \quad D = D'/R \quad \text{and} \quad V_p = V_p'/\Omega^* R, \qquad [4]$$

where $2D$ is the dimensionless cylinder center-to-center distance and $2L$ is the dimensionless separation distance between the parallel plates. $V_p$ is the dimensionless velocity of the moving plates; because in the absence of cylinders $V_p' = GL'$, $G$ being the rate of shear, one can identify $\Omega^*$ by $G$.

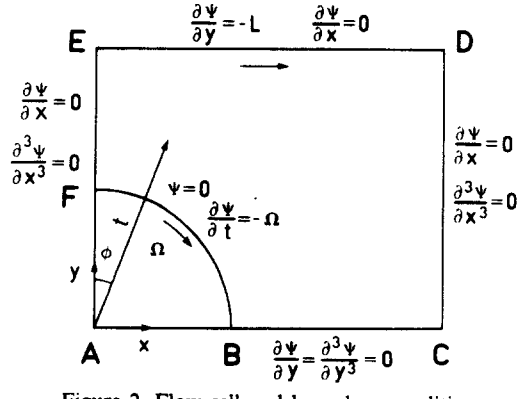


Figure 2. Flow cell and boundary conditions.

The flow cell representing the flow is shown in figure 2. Analogous to the flow past a periodic array of cylinders (Sangani & Acrivos 1982), due to the symmetry of the flow, only the flow region BCDEF need be considered. The plates' velocity $V_p$ was restricted to a value $L$. This means that in the absence of the cylinders, the velocity field between the parallel plates is given by a simple shear flow, namely $v_x = y$. Due to the linearity of the flow, setting $V_p = L$ does not reduce the generality of the flow problem.

The appropriate boundary conditions are given as:

on BF $$\psi = 0, \quad \frac{\partial \psi}{\partial x} = -\Omega \quad \text{or} \quad \zeta = \frac{\partial^2 \psi}{\partial r^2} - \frac{\Omega}{r}; \tag{5a}$$

on BC $$\frac{\partial \psi}{\partial y} = 0, \quad \frac{\partial^3 \psi}{\partial y^3} = 0 \quad \text{or} \quad \frac{\partial \zeta}{\partial y} = 0; \tag{5b}$$

on DC $$\frac{\partial \psi}{\partial x} = 0, \quad \frac{\partial^3 \psi}{\partial x^3} = 0 \quad \text{or} \quad \frac{\partial \zeta}{\partial x} = 0; \tag{5c}$$

on DE $$\frac{\partial \psi}{\partial y} = -L, \quad \frac{\partial \psi}{\partial x} = 0 \quad \text{or} \quad \zeta = \frac{\partial^2 \psi}{\partial y^2}; \tag{5d}$$

and

on EF $$\frac{\partial \psi}{\partial x} = 0, \quad \frac{\partial^3 \psi}{\partial x^3} = 0 \quad \text{or} \quad \frac{\partial \zeta}{\partial x} = 0. \tag{5e}$$

Since the cylinders are free to rotate, their angular velocity $\Omega(=\Omega'/\Omega^*)$ is determined by the condition of zero hydrodynamic couples acting on them, i.e.

$$\int_0^{2\pi} r^2 \left( \frac{\partial^2 \psi}{\partial r^2} - \frac{1}{r} \frac{\partial \psi}{\partial r} - \frac{1}{r^2} \frac{\partial^2 \psi}{\partial \phi^2} \right) d\phi = 0. \tag{6}$$

The stream function derivatives are related to the velocity:

$$v_x = -\frac{\partial \psi}{\partial y}, \quad v_y = \frac{\partial \psi}{\partial x}, \quad v_r = \frac{1}{r} \frac{\partial \psi}{\partial \phi}$$

and

$$v_\phi = -\frac{\partial \psi}{\partial r}.$$

The velocities are rendered dimensionless by $(\Omega^* R)$.

The shear stress, $\tau_{r\phi}$, is given by

$$\tau_{r\phi} = -\left( \frac{\partial v_\phi}{\partial r} - \frac{v_\phi}{r} + \frac{1}{r} \frac{\partial v_r}{\partial \phi} \right). \tag{7}$$

The shear stress is rendered dimensionless using $\tau_{r\phi} = \tau'_{r\phi}/\mu_0 \Omega^*$, where $\mu_0$ is the fluid viscosity. At the cylinder surface, the shear stress and the vorticity at the surface are given by

$$\tau_{r\phi} = \frac{\partial^2 \psi}{\partial r^2} + \Omega \tag{8a}$$

and

$$\zeta = \frac{\partial^2 \psi}{\partial r^2} - \Omega, \tag{8b}$$

respectively. Equations [8a,b] lead to

$$\tau_{r\phi} = \tau_c = \zeta + 2\Omega \tag{9}$$

where $\tau_c$ is local shear stress at the cylinder surface. Along the moving plates, the plate local shear stress, $\tau_p$, is given by

$$\tau_p = \zeta. \quad [10]$$

The average shear stress, $\langle \tau_p \rangle$, is given by

$$\langle \tau_p \rangle = \frac{1}{D} \int_0^D \tau_p \, dx. \quad [11]$$

As discussed above, one can think of the flow system, where a single row of cylinders is sheared by two parallel plates, as being a simplified case of a suspension or ordered cylinders undergoing simple shear. To this end, it is possible then, to relate the suspension viscosity $\mu_s$ by

$$\frac{\mu_s}{\mu_0} = \langle \tau_p \rangle \quad [12]$$

where, in the absence of the cylinders, the average shear stress on the plate is unity. Equation [12] becomes useful in assessing the value of the viscosity ratio $\mu_s/\mu_0$ for different geometries, i.e. cylinder spacing, parallel-plate gap width and concentration.

## METHODS OF SOLUTION

Two methods of solution were attempted: a finite-difference method and a least-squares technique. Both solution methods are complimentary to each other and they served as a check to the accuracy of the results.

In the finite-difference method, [3a,b] was solved. The surface vorticity was approximated using a Taylor series expansion up to and including the third derivative of $\psi$ in a manner similar to Masliyah & Epstein (1970). A rectangular grid mesh was used with interpolation at the cylinder surface. The interpolation scheme was an adaptation of that given by Gordon (1978). A Gauss–Seidel point iterative scheme was used to solve the discretized form of [3a,b] for a given value of $\Omega$ at the cylinder surface. Once a converged solution was obtained, the integral of [6] was evaluated using a cubic spline. The value of $\Omega$ was readjusted till the converged solution of [6] gave a torque value of $< 10^{-2}$.

In the method of least squares, use is made of the general solution of [1]. The general solution that satisfies the boundary conditions along BC and EF is given by

$$\psi = f_0 + \sum_1^\infty f_n \cos 2n\phi, \quad [13]$$

where

$$f_0 = \mathrm{A}\, r^2 \ln r + \mathrm{B}\, r^2 + \mathrm{C} \ln r + \mathrm{D} \quad [14]$$

and

$$f_n = a_n r^{2n+2} + b_n r^{2n} + c_n r^{-2n+2} + d_n r^{-2n}. \quad [15]$$

In order to satisfy the zero torque condition given by [6] and $\psi = 0$ at the cylinder surface, it can be shown that

$$\mathrm{A} = \mathrm{C} = 0, \quad \mathrm{B} = -\frac{\Omega}{2} \quad \text{and} \quad \mathrm{D} = \frac{\Omega}{2}. \quad [16]$$

Making use of the boundary conditions along FB leads to

$$c_n = -(2n+1)a_n - 2nb_n \quad [17a]$$

and

$$d_n = 2na_n + (2n-1)b_n. \quad [17b]$$

Combining [15]–[17b] with [13] leads to

$$\psi = -\tfrac{1}{2}\Omega(r^2-1) + \sum_{1}^{N}\{a_n[r^{2n+2} - (2n+1)r^{-2n+2} + 2nr^{-2n}] + b_n[r^{2n} - 2nr^{-2n+2} + (2n-1)r^{-2n}]\}\cos 2n\phi. \quad [18]$$

Equation [18] satisfies all the boundary conditions, except those along ED and DC. The coefficients $a_n$ and $b_n$ together with $\Omega$ are to be determined in such a manner as to satisfy the boundary conditions along ED and DC in a "least-square average" sense (Sangani & Acrivos 1982). This is accomplished by choosing $M$ points ($M > N$) along ED and DC. At each point two boundary conditions are to be satisfied. Therefore, $2M$ equations are generated with $2N+1$ unknowns. This overdetermined set of equations is reduced to a system of $2N+1$ equations with $2N+1$ unknowns using the method of least squares, which is described by Lapidus (1962) and Forsythe *et al.* (1977). Once the unknowns, $\Omega$, $a_n$ and $b_n$ are determined, it is then possible to evaluate the velocity field and the surface shear stress via the surface vorticity.

In general it was found that by choosing $M = 45$ and $N = 35$, the value of $\Omega$ becomes insensitive (within $10^{-4}$) to higher values of $M$ and $N$. In all cases, the matrix condition was used as a guide to determine the optimal value of $M$ and $N$. The maximum deviation in the value of $\Omega$ between the least-squares method and the finite-difference method was about 4%.

## LIMITING SOLUTIONS

In the case of a single cylinder in a shear flow, i.e. $L$ and $D \to \infty$, Cox *et al.* (1968) showed that the solution is given by setting $N = 1$ in the general solution given by [18]. Their stream function $\psi$ is given by

$$\psi = -\tfrac{1}{4}(r^2-1) + (r^2 - 2 + r^{-2})\cos 2\phi \quad [19]$$

and

$$\Omega = \tfrac{1}{2}. \quad [20]$$

The shear stress at the cylinder surface is then given by

$$\tau_{r\phi} = 2\cos 2\phi. \quad [21]$$

The solution of Cox *et al.* (1968) gives the upper limit of the angular velocity of a cylinder placed in a simple shear flow. This limit is given by [20].

For the case of a small gap between a single cylinder rotating with an angular velocity $\Omega$ near a wall moving with a velocity $V_p$, analysis using lubrication theory can be shown to give

$$Q = \tfrac{2}{3}\Delta(\Omega + V_p) \quad [22]$$

and

$$\Omega = V_p\frac{\sqrt{2\Delta}}{\pi}, \quad [23]$$

where $\Delta$ is the dimensionless gap between the cylinder surface and the plate and $Q$ is the dimensionless flow rate between the cylinder and the moving plate ($Q = Q'/R\Omega^*$). In this analysis $V_p$ is restricted to a value of $L$. In the limit of a small gap, $\Delta \to 0$, $L \to 1$ and [22] and [23] show that both $Q$ and $\Omega$ approach zero when the cylinder touches the plate. The limiting cases of an isolated cylinder in a simple shear flow and that of a cylinder near a moving plate serve as a check to the numerical analysis, which in turn can be used to establish the limits of their validity.

## DISCUSSION OF RESULTS

It was pointed out earlier that two methods of solution were employed. The finite-difference method was capable of handling all values of $L/D$, albeit, that the computational demand was fairly high. The computational demand of the least-squares method was much less; however it suffered from producing a matrix having a high condition number which could cast some doubt on the numerical accuracy of the results (Forsythe *et al.* 1977). This was especially the case for either an $L/D$-value higher than 3 or lower than 1/3. In all cases tested, the results from both methods of solution were normally within 1–2% and at worst 4% from each other. The grid size for the finite-difference method varied from 0.01 to 0.1.

Figure 3a–f show the contours of the stream function at a fixed $L$-value of 1.3 for different $D$-values. At a large value of $D$ ($=3$), figure 3a shows a critical closed streamline

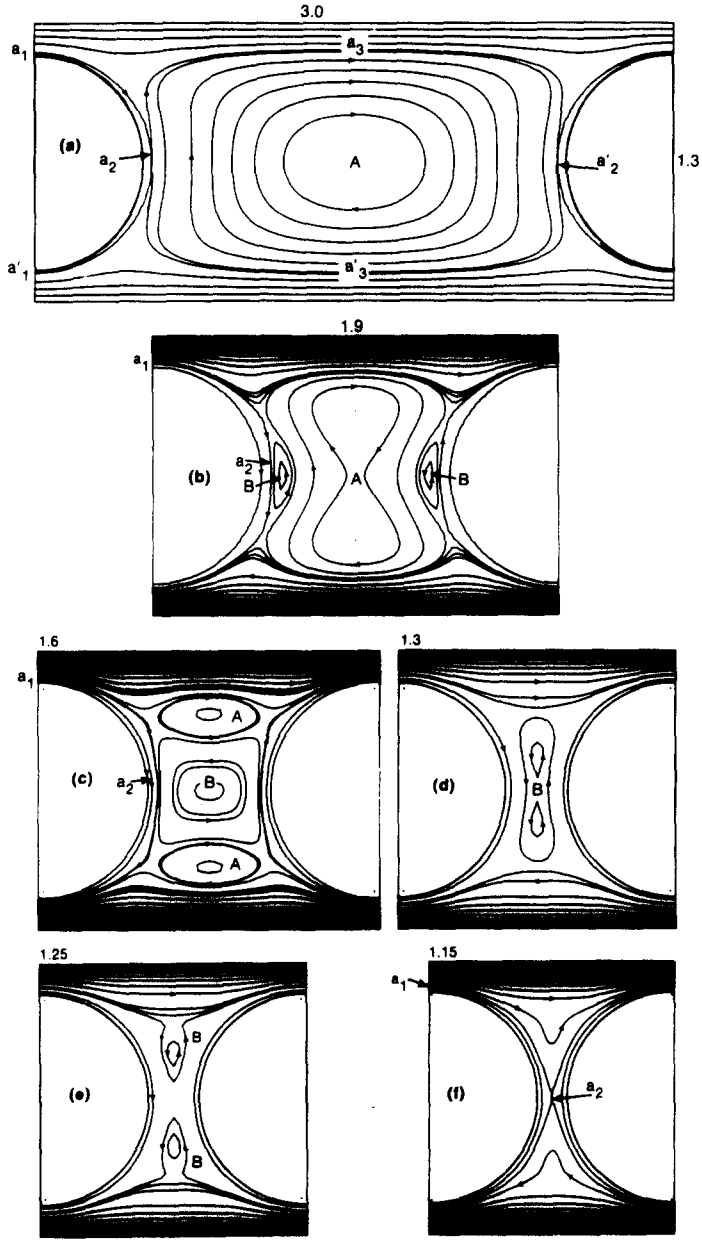


Figures 3a–f. Contours of the stream function for $L = 1.3$: (a) $L/D = 0.433$; (b) $L/D = 0.684$; (c) $L/D = 0.812$; (d) $L/D = 1.00$; (e) $L/D = 1.04$; (f) $L/D = 1.13$.

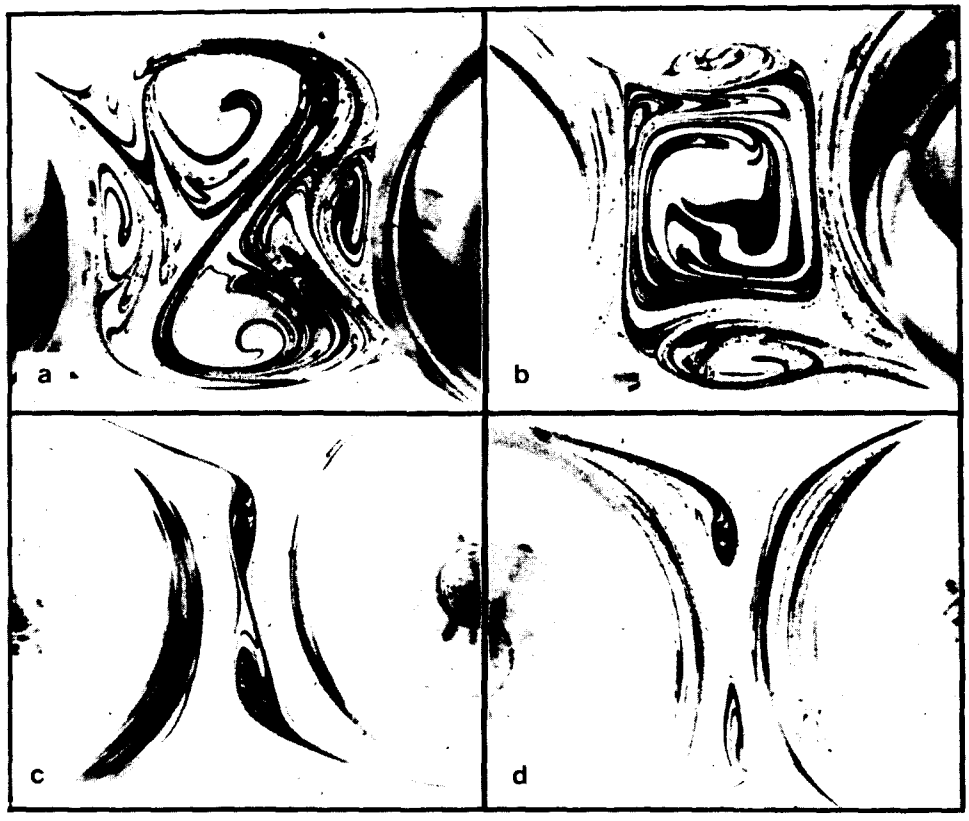


Figures 4a–d. Experimental flow patterns for $L = 1.315$: (a) $L/D = 0.68$; (b) $L/D = 0.80$; (c) $L/D = 0.99$; (d) $L/D = 1.02$.

$a_1a_2a_1'$. Any fluid between the cylinder and the streamline $a_1a_2a_1'$ circulates around the cylinder and remains entrapped. Similarly, streamline $a_2a_3a_2'a_3'$ bounds the fluid that circulates within the central core. For clarity let this vortex be denoted by A. The fluid between the moving plate and streamline $a_1a_2a_3$ is free to move from one cell to another. On reducing the cylinder center-to-center distance to $D = 1.9$ (figure 3b), a new vortex close to the cylinder emerges. Let this vortex be denoted by B. Its circulation direction is opposite to the central core vortex, A. The critical streamline $a_1a_2$ remains nearly unchanged. On further decreasing $D$, figure 3c shows that vortex B grows at the expense of vortex A. On further reduction in $D$, from 1.6 to 1.3, figure 3d shows that vortex A disappears and vortex B occupies the central core. Decreasing $D$ from 1.3 to 1.25, figure 3e shows that vortex B becomes smaller and splits up into two vortices away from the centerline of the plates. Finally, on further reducing $D$ to 1.15, figure 3f, vortex B disappears and point $a_2$ of the critical streamline reaches the center of the flow cell.

It will be mentioned at a later stage that flow visualization experiments were conducted. Figures 4a–d show the streamlines from these flow visualization experiments. Clearly figures 4a–d correspond to figure 3b–e, respectively. It is clear from figures 3a–f and 4a–d that the effect of the cylinder center-to-center distance has a profound influence on the flow pattern.

The effect of the plate spacing on the flow field at a fixed value of $D = 3$ is shown in figures 5a–e. For a small plate spacing, $L = 1.1$, a vortex was found near the cylinder similar to the case of $L = 1.3$ and $D = 1.9$ of figure 3b. Also a central core vortex is present. On increasing the plates spacing the vortex close to the cylinder disappears. With the increase of the plates spacing, the central core vortex becomes smaller until it completely disappears, as shown in figure 5e for the case of $L = 4$. The critical streamline $a_1a_2$ occupies a large region of the flow field.

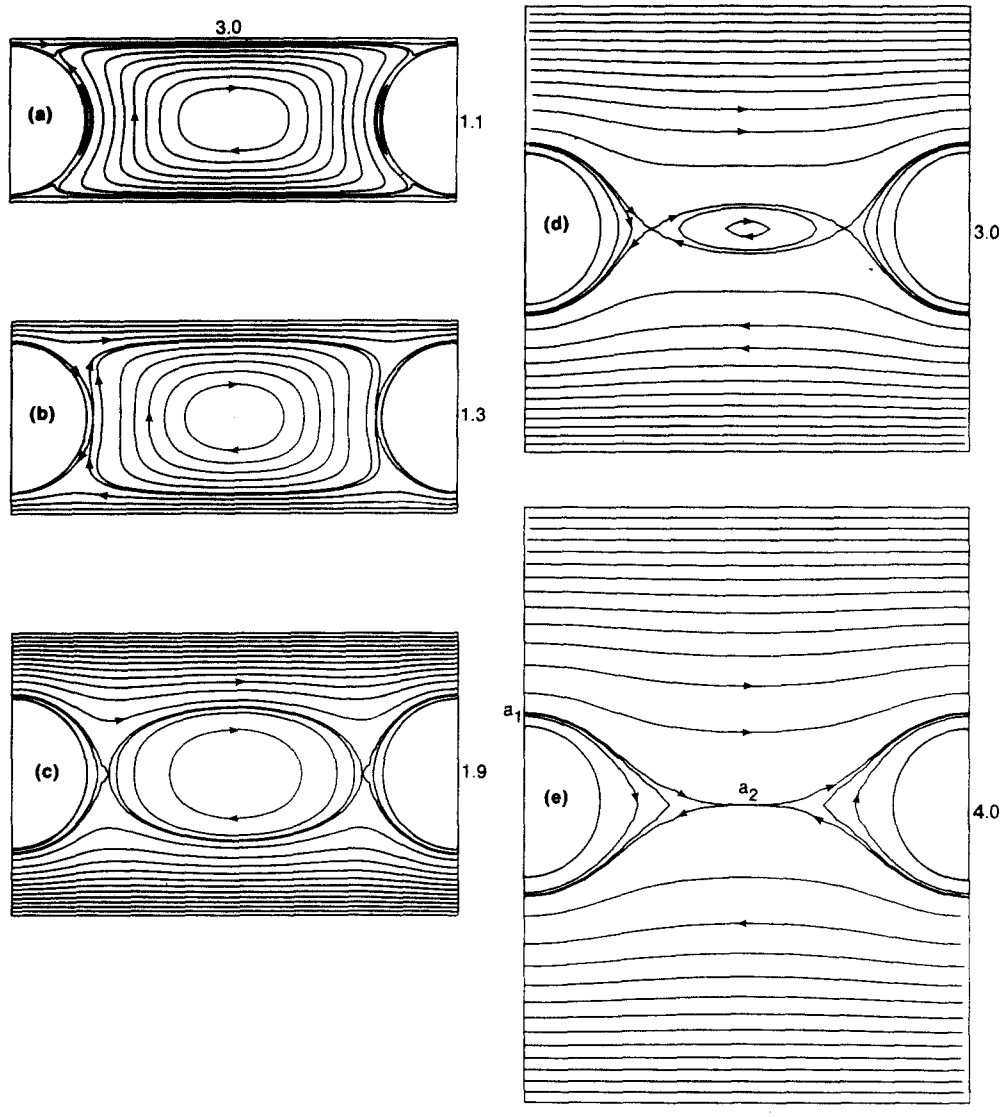


Figures 5a–e. Contours of the stream function for $D = 3$.

The variation of the angular velocity of the cylinder with the ratio of plate spacing to cylinder center-to-center distance, $L/D$ is shown in figure 6 for various values of $LD$. The product $LD$ can be thought of as being a measure of the concentration of the cylinders, where the cylinder concentration is given by

$$c = \frac{\pi \frac{R^2}{4}}{L'D'} = \frac{\pi}{4LD}.$$

At large values of $LD$ the system is considered to be dilute. For $LD = 50$ and $L/D$ close to unity, the value of $\Omega$ is close to 0.5, which is the theoretical value as $LD \to \infty$, as given by Cox *et al.* (1968). For a given value of $LD$, the value of $\Omega$ becomes zero in the limiting case of $D \to 1$ and $L \to 1$. In the limit of $D = 1$, the cylinders touch each other and hence are prevented from rotating. This limiting case does not represent any conceptual difficulties. In the case of $L \to 1$, the moving plates touch the cylinders, whereby the cylinder comes into contact with the moving plates but it does not rotate. In real systems this cannot be true as other phenomena become important as the gap $\Delta(=L-1)$ between the cylinders and the plates becomes small. For example, cavitation occurs when the gap width is very small and the effects of surface roughness also become important.

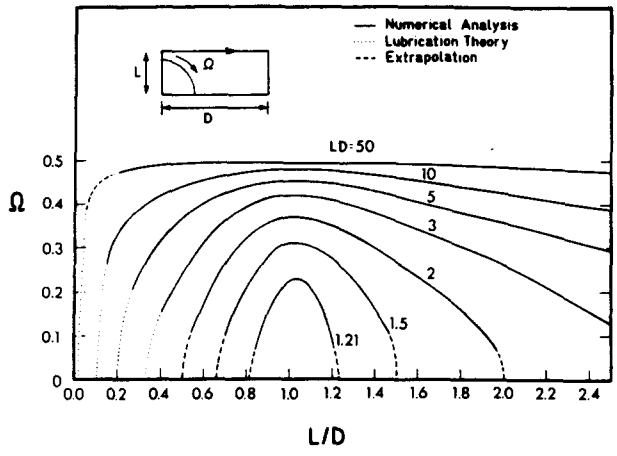


Figure 6. Variation of the cylinder angular velocity with $L/D$.

For the case of large $LD$ and small gap, $\Delta$, it is possible to analyze the present flow using lubrication theory. Using classical lubrication theory (Langlois 1964), one can show that for an isolated cylinder near a moving wall, the cylinder angular velocity is given by [23] and the flow rate between the moving plate and the cylinder is given by [22]. Comparison between [22] and [23] with the numerical results of this study is shown in table 1. For low values of the gap width, $\Delta$, the agreement between the lubrication theory and the numerical results is remarkably good.

The variation of the velocity in the $x$-direction, $v_x$, is shown in figures 7 and 8 for two different geometries. For the case of $L = 1.9$ and $D = 2$, the velocity, $v_x$, variation along $x = 0$ and $x = 2$ is monotonic, as is shown in figure 7. Along $x = 0$ at $y = 1.9$, the value of the velocity is that of the moving plate and at $y = 1$ it is given by the value of $\Omega$. Along $x = 1.9$ the velocity deviates appreciably from the straight line $v_x = y$ which is the velocity variation for the case of $D \to \infty$. For the case of $L = 1.3$ and $D = 3$, the velocity, $v_x$, profile is shown in figure 8. An important feature in the $v_x$-variation along $x = 0$ is that $dv_x/dy$ changes sign close to the moving plate. In other words, the fluid velocity, $v_x$, is not maximum at the moving plate itself. This, of course, leads to positive and negative local shear stresses along the moving plate for $x \cong 0.0$. This will be shown to be the case. Along $x = 3$, the variation of $v_x$ is nearly that of $v_x = y$, showing little effect due to the presence of the cylinders within the parallel plates.

The variation of the shear stress, $\tau_p$, along the plate is given in figures 9 and 10. For $L = 1.3$, figure 9 shows the plate shear stress variation for different values of $D$. For large cylinder center-to-center distance, $D = 3$, the plate shear stress near $x = 0$ is negative, reaches a maximum at about $x = 0.85$, and then levels off to a value of unity for $x > 4$. The negative shear stress near $x = 0$ is due to the shape of the $v_x$-profiles, where the velocity $v_x$ is maximum away from the plate. In the absence of the cylinders, the shear stress is uniform and is equal to unity. The approach of $\tau_p$ to unity for $x > 4$ indicates that at the outflow boundary, $x = 5$, the flow is not influenced by the presence of the cylinders. For

Table 1. Comparison between various numerical methods and asymptotic solution

| | | $\Omega$ | | | $Q$ | | |
|---|---|---|---|---|---|---|---|
| $\Delta$ | $V_p = L$ | [23] | FDM[a] | LSM[a] | [22] | FDM | LSM |
| 1.0 | 2 | 0.900 | 0.435 | 0.430 | 1.93 | 1.41 | 1.46 |
| 1.0 | 1.3 | 0.320 | 0.262 | 0.273 | 0.343 | 0.303 | 0.306 |
| 0.15 | 1.15 | 0.200 | 0.191 | 0.197 | 0.138 | 0.133 | 0.133 |
| 0.1 | 1.10 | 0.157 | 0.153 | 0.158 | 0.0838 | 0.083 | 0.083 |

[a]FDM = finite-difference method, LSM = least-squares method.

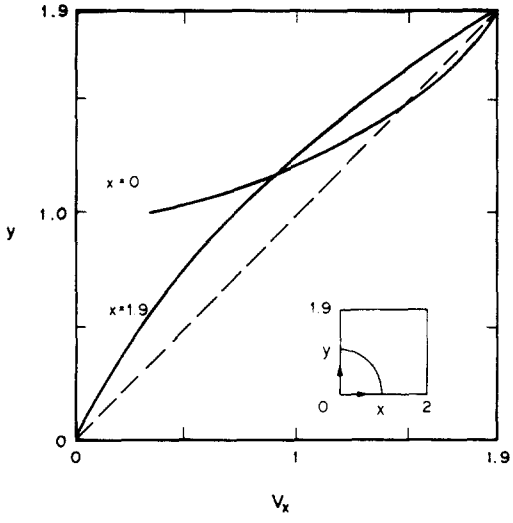


Figure 7. Fluid velocity variation in the $x$-direction for $L = 1.9$ and $D = 2$.

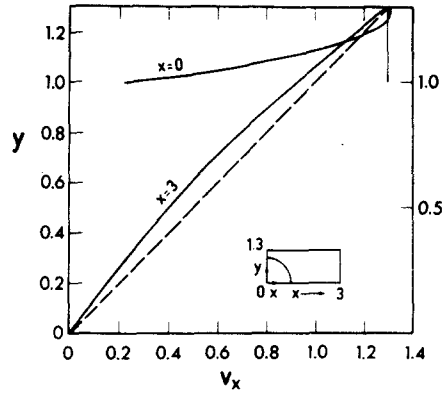


Figure 8. Fluid velocity variation in the $x$-direction for $L = 1.3$ and $D = 3$.

the cases of $D = 2$ and $D = 3$, the shear stress variation with $x$ is identical to the case of $D = 5$ when $x$ approaches the outflow region of the cell. However, for $D = 1.3$ and $D = 1.15$ it is positive for all $x$-values.

The shear stress variation along the plate at $D = 3$ for various values of $L$ is shown in figure 10. For low values of $L$, there is a large variation of $\tau_p$ along the plate. The location of the maximum value of $\tau_p$ shifts towards the cell outflow region as $L$ is increased.

The variation of the shear stress, $\tau_c$, at the cylinder surface is shown in figure 11. In the limit of large $L$ and $D$, the expression by Cox *et al.* (1968) for the stream function can be used to evaluate the value of $\tau_c$ which is given by

$$\tau_c = 2 \cos 2\phi.$$

The deviation from the above expression is most pronounced when $L$ is small. For the case of $L = 2.5$ and $D = 3.0$, the $\tau_c$-variation is shown to be fairly close to the expression of Cox *et al.* (1968).

It was pointed out earlier that the flow system of a row of cylinders sheared between two parallel plates represents an idealized suspension of cylinders. The viscosity ratio $\mu_s/\mu_0$ represents the effect of the presence of the cylinders in the shear flow and its values can

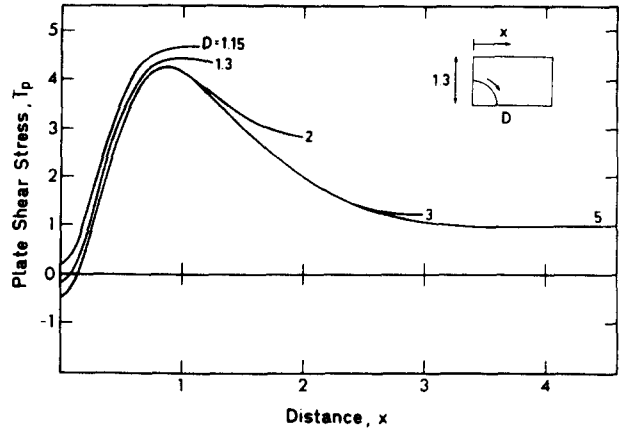


Figure 9. Variation of the plate shear stress for $L = 1.3$.

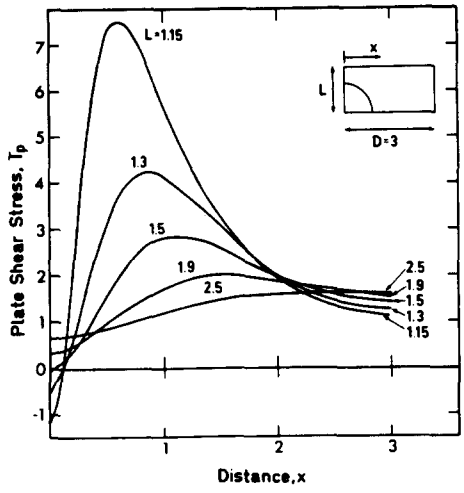


Figure 10. Variation of the plate shear stress for $D = 3$.

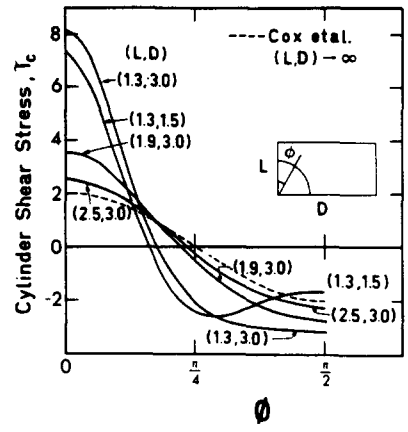


Figure 11. Variation of the cylinder shear stress.

be evaluated using [10]–[13]. Figure 12 shows the variation of $\mu_s/\mu_0$ with $L/D$ for various $LD$-values. For large $LD$-values, i.e. low suspension concentration, $\mu_s/\mu_0$ is little affected by the $L/D$ ratio. However, for low values of $LD$, i.e. at high suspension concentration, the dependence of $\mu_s/\mu_0$ on $L/D$ becomes very significant with $\mu_s/\mu_0$ increasing with a decrease in $L/D$. This means that for a given suspension concentration, the viscosity ratio $\mu_s/\mu_0$ is lower when the cylinders are stacked close to each other (i.e. small $D$ and large $L$). This is in qualitative agreement with observations on sheared suspensions of ordered lattices (Tomita & van de Ven 1984) which show an increase in spacing (i.e. in $L$) between the sliding layers and an increase of the number of particles in each layer (i.e. a decrease in $D$). However, in such systems the flow behavior is complicated by the presence of diffusive ionic double layers around the particles.

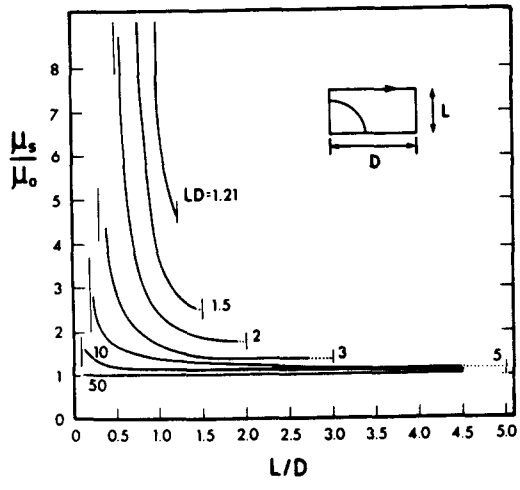


Figure 12. Viscosity ratio variation with $L/D$.

## EXPERIMENTAL SETUP AND PROCEDURE

The experimental study was aimed towards flow visualization and measurements of the angular velocity of the cylinders. The experimental investigation was carried out using a Couette device. It consisted of two accurately machined concentric counter-rotating

Table 2. Characteristics of the experimental setup

| | |
|---|---|
| Inner cylinder radius | 12.63 cm |
| Outer cylinder radius | 15.30 cm |
| Couette gap | 2.63 cm |
| Depth of Couette cylinder | 14 cm |
| Test cylinder radius | 1.00 cm |
| Test cylinder length | 7.50 cm |
| Silicone oil viscosity | 10 Pa s |

vertical lucite cylinders, each of which is driven by a continuously variable-speed motor whose speed can be controlled to 0.2% or better. A full description of the Couette device is given elsewhere (Darabaner *et al.* 1967). Electronic frequency counters were used to monitor the rotational speed of the Couette cylinders. The inner and outer cylinders were to rotate at the same peripheral velocity in opposite directions. Silicone oil having a high viscosity was placed in the annulus of the Couette device and used as the working fluid. In the experimental study, the inner and outer surfaces of the concentric cylinders simulate the moving plates.

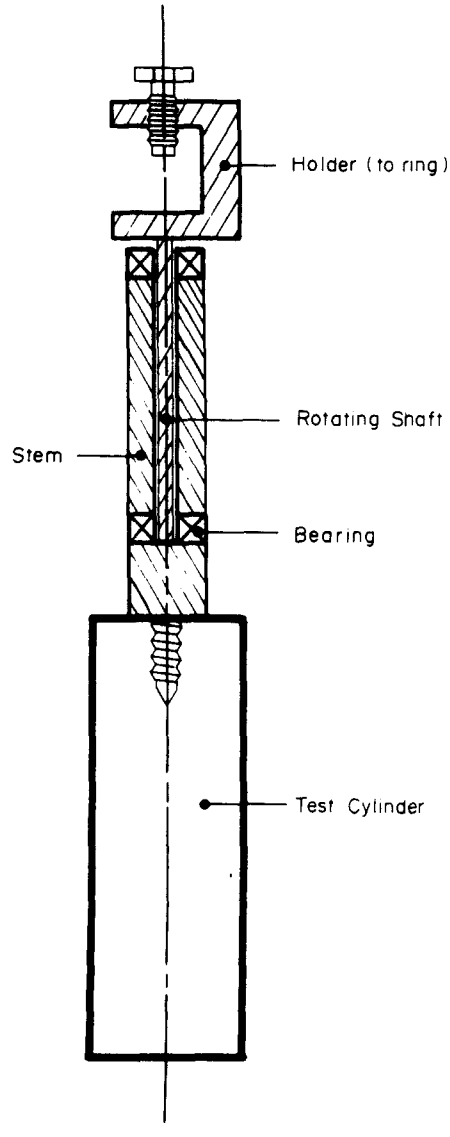


Figure 13. Rotating test cylinder.

To simulate the array of parallel cylinders, five cylinders were constructed. Each cylinder rotated freely about its axis. Figure 13 shows a typical cylinder with its rotating shaft and holder. The cylinders were attached via their holders to a common rigid ring that was placed at the centerline of the Couette annulus. The cylinder center-to-center distance was adjusted by moving the cylinder holder along the ring. The distance between each cylinder was measured using spacer blocks. Table 2 gives the dimensions of the Couette device and those of the cylinders.

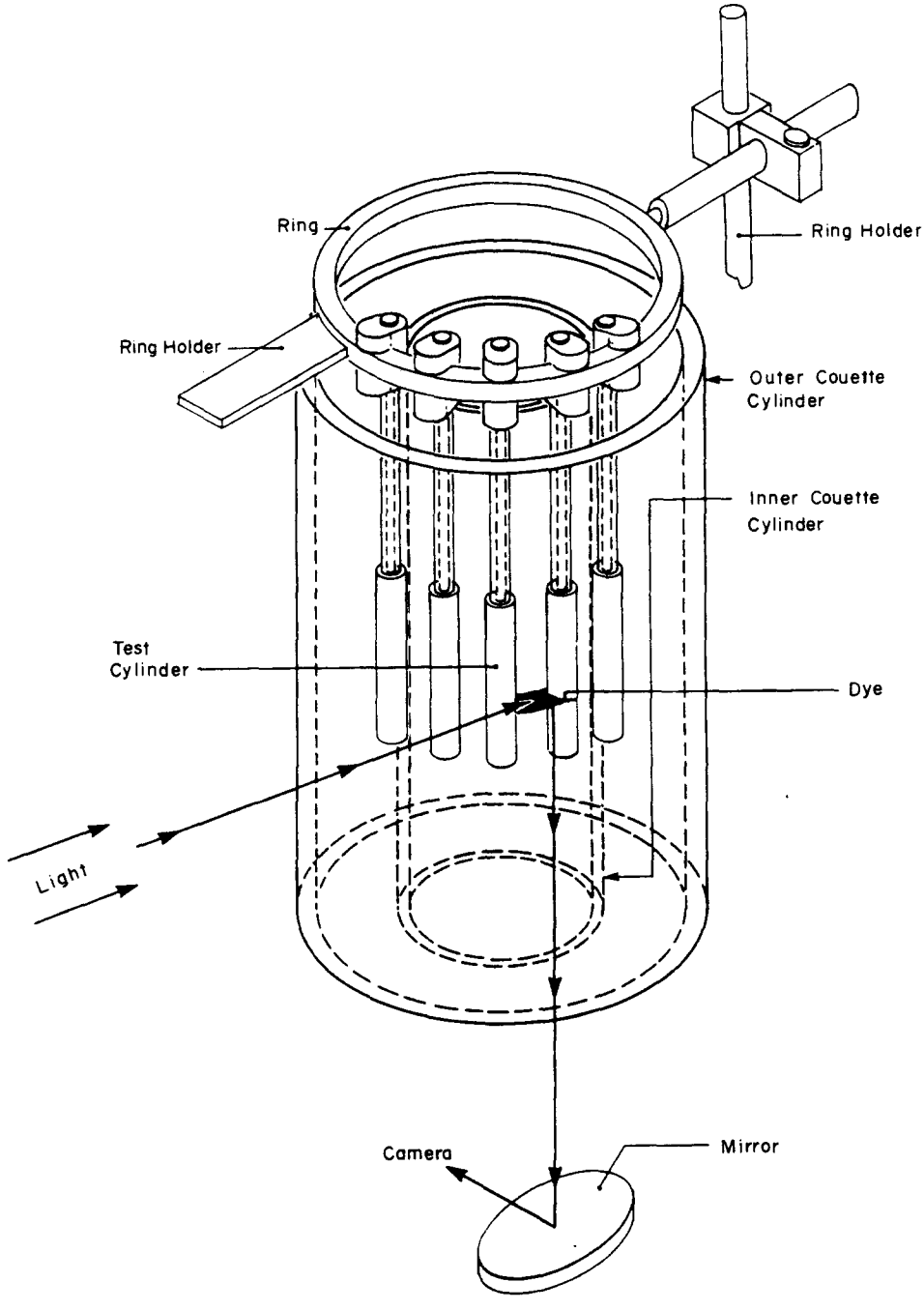


Figure 14. Experimental setup (schematic). The five test cylinders are connected to a ring with a diameter corresponding to the center of the gap between the Couette cylinders. The ring is held in place by a ring holder that, using several adjustable screws, allows precise positioning of the test cylinders into the annular gap. Streamlines were made visible by using a fluorescent dye placed between the two central tests cylinders and were photographed from below.

The five cylinders were placed in the Couette annulus to isolate the cylinder with the least rotational bearing friction. The velocity of the Couette cylinders was first set at a high value and it was gradually reduced. Four of the cylinders stopped rotating when the Couette cylinder peripheral speed was about $V' = 0.4$ cm/s, and the fifth cylinder stopped rotating at $V' = 0.1$ cm/s. The fifth cylinder having the least bearing friction was used as the test cylinder and was placed in the center of the cylinder row. All measurements were made on the test cylinder and in the space adjacent to it. A schematic presentation of the experimental setup is shown in figure 14.

## EXPERIMENTAL RESULTS

Flow visualization was made using a red fluorescent dye. It was prepared by dissolving the dye in the working silicone oil and using the dye solution as the tracer in the flow visualization experiments. Intense cold light transmitted via a fiber optic was used for illumination. Due to the high viscosity of the silicone oil, the free surface of the oil gave a high surface distortion. As the bottom of the Couette apparatus was transparent, flow visualization was made from the bottom of the Couette apparatus.

With the Couette cylinders stationary, the dye was introduced to the gap around the test cylinder using a long fine-stem disposable pipette. The Couette cylinders were then rotated at a velocity of 2.4 cm/s. Once a flow pattern was established, the Couette cylinders were stopped and the flow pattern generated by the dye was photographed. The flow patterns shown in figures 4a–d are in excellent qualitative agreement with the streamlines generated numerically.

The variation of the cylinder angular velocity was measured for a fixed value of $L$ which is imposed by the annulus width of the Couette cylinders. For a given value of the cylinder center-to-center distance and the Couette cylinders velocity, the angular velocity of the test cylinder was measured by recording the time taken for a line mark on the stem of the test cylinder to rotate a specified number of times. For a given cylinder center-to-center distance, the variation of the cylinder angular velocity was found to be proportional to the Couette cylinder velocity, as is shown in figure 15. This is quite reasonable as the test cylinder stopped rotating after a relatively small value of $V'_p$, indicating that the bearing friction is quite low. The value of $\Omega = (\Omega'/\Omega^*)$ is given by $SL'R\Omega^*$ where, in this case, $R = 1$ cm, $\Omega^* = 1\ s^{-1}$ and $L' = 1.315$ cm. The quantity $S$ is the slope of $\Omega'$ vs $V'_p$. Comparison between the experimental and theoretical results for the cylinder angular velocity is shown in figure 16. The experimental results are for the case where the silicone-free surface is just below the test cylinder, a situation where the end effects are lowest. In general, good agreement was found between the experimental and theoretical angular velocities, especially for $L/D > 1$. At low values of $L/D$, the effect of curvature present in the Couette flow becomes more significant and more deviation would be expected between the flow within parallel flat plates and concentric cylinders.

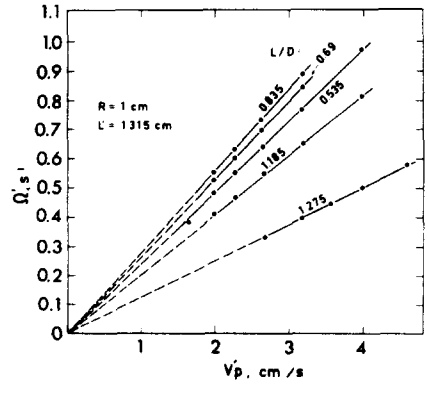


Figure 15. Variation of the cylinder angular velocity with plate velocity.

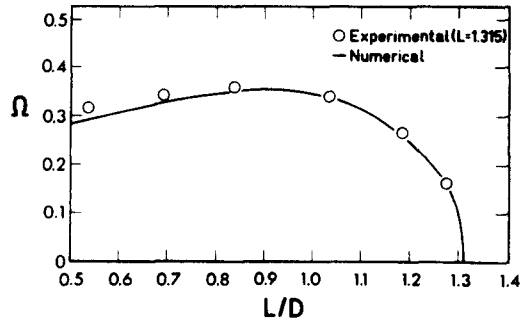


Figure 16. Variation of the cylinder angular velocity with $L/D$ at $L = 1.315$.

In order to gain an appreciation of the error in measurement due to end effects, measurements were made with the silicone-oil-free surface 2.5 cm below the upper end of the test cylinder. This represents one-third of the available length of the test cylinder. Measurements in $\Omega$ were affected by about $\pm 3\%$, indicating that the end effects were not very significant.

During our experiment we observed another interesting phenomenon. In previous experiments with the Couette apparatus, we usually had a layer of glycerol on the bottom of the apparatus in order to minimize the effects of the bottom plate on the velocity profile in the gap between the two cylinders. In the experiments described in this paper, this layer was absent but it was present in preliminary experiments. We observed some very spectacular three-dimensional fluid motion in which the glycerol moved upwards, sometimes up to half the height of the cylinders, in a complex but reproducible fashion. This shows that introducing a new phase greatly complicates the fluid motion.

## CONCLUDING REMARKS

It has been shown that even a rather simple system of an array of cylinders subjected to shear shows a surprisingly rich variety of flow patterns. This implies that the flow in sheared concentrated ordered suspensions must be quite complex. In this paper we have established the various flow patterns that can occur in a sheared array of aligned cylinders and calculated the shear stresses exerted on the boundaries and the cylinders. We also predicted the angular velocity of the cylinders as a function of volume fraction and spacing. Experiments on a row of five cylinders confirm the general features of the theory, especially the occurrence of the various flow patterns and the variation of angular velocity with spacing.

The two-dimensional model of ordered suspensions of cylinders is a simple example of an ordered structure subjected to shear. It qualitatively explains some of the observations in ordered suspension that are subjected to shear such as restructuring in fewer more densely packed layers together with a reduction in viscosity (shear thinning behavior).

*Acknowledgement*—One of the authors (J.H.M.) is grateful to the Natural Sciences and Engineering Research Council of Canada for financial support in providing a Senior Industrial Fellowship while on study leave.

## REFERENCES

ADLER, P. M. & BRENNER, H. 1985 Spatially periodic suspensions of convex particles in linear shear flows. I. Description and kinematics. *Int. J. Multiphase Flow* **11,** 361–385.

ADLER, P. M., ZUZOVSKY, M. & BRENNER, H. 1985 Spatially periodic suspensions of convex particles in linear shear flows II. Rheology. *Int. J. Multiphase Flow* **11,** 387–417.

ALDER, B. J., HOOVER, W. G. & YOUNG, D. A. 1968 Studies in molecular dynamics. V. High density equation of state and entropy for hard disks and systems. *J. chem. Phys.* **44,** 3688–3696.

COX, R. G., ZIA, I. Y. Z. & MASON, S. G. 1968 Particle motions in sheared suspensions. XXV. Streamlines around cylinders and spheres. *J. Colloid Interface Sci.* **27,** 7–18.

DARABANER, C. L., RAASCH, J. K. & MASON, S. G. 1967 Particle motions in shear suspensions. XX. Circular cylinders. *Can. J. chem. Engng* **45,** 3–12.

FORSYTH, P. A., MERVCELJA, S. JR, MITCHELL, D. J. & NINHAM, B. W. 1978 Ordering in colloidal systems. *Adv. Colloid Interface Sci.* **9,** 37–60.

FORSYTHE, G. E., MALCOME, A. & MOLER, C. B. 1977 *Computer Methods for Mathematical Computations*. Prentice-Hall, Englewood Cliffs, N.J.

GORDON, D. 1978 Numerical calculations on viscous flow fields through cylinder arrays. *Comput. Fluids* **6,** 1–13.

HILTNER, P. A., PAPIR, Y. S. & KRIEGER, I. M. 1971 Diffraction of light by non-aqueous ordered suspensions. *J. phys. Chem.* **75,** 1881–1886.

HOFFMAN, R. L. 1974 Discontinuous and dilatant viscosity behavior in concentrated suspensions. II. Theory and experimental tests. *J. Colloid Interface Sci.* **46,** 491–506.

LANGLOIS, W. E. 1964 *Slow Viscous Flow.* Macmillan, New York.

LAPIDUS, L. 1962 *Digital Computation for Chemical Engineers.* McGraw-Hill, New York.

MASLIYAH, J. H. & EPSTEIN, N. 1970 Numerical study of steady flow past spheroids. *J. Fluid Mech.* **44,** 493–512.

ONSAGER, L. 1949 The effects of shape on the interaction of colloidal particles. *Ann. N.Y. Acad. Sci.* **51,** 627–659.

OSTER, G. 1950 Two-phase formation in solutions of tobacco mosaic virus and the problem of long range forces. *J. gen. Physiol.* **33,** 445–473.

SANGANI, A. S. & ACRIVOS, A. 1982 Slow flow past periodic arrays of cylinders with application to heat transfer. *Int. J. Multiphase Flow* **8,** 193–206.

TOMITA, M. & VAN DE VEN, T. G. M. 1984 The structure of sheared ordered latices. *J. Colloid Interface Sci.* **99,** 374–386.

TOMITA, M., TAKANO, K. & VAN DE VEN, T. G. M. 1983 An optical method for studying the properties of ordered lattices. *J. Colloid Interface Sci.* **92,** 367–382.

VAN DE VEN, T. G. M. 1985 The flow of suspensions. *Polym. Composites* **6,** 209–214.

ZUZOVSKY, M., ADLER, P. M. & BRENNER, H. 1983 Spatially periodic suspensions of convex particles in linear shear flows. III. Dilute arrays of spheres suspended in Newtonian fluids. *Physics Fluids* **26,** 1714–1723.